The Taurid Resonant Swarm at Mercury

Apostolos A. Christou, Auriane Egal, Nikolaos Georgakarakos

Monthly Notices of the ROYAL ASTRONOMICAL SOCIETY

MNRAS **527,** 4834–4846 (2024) https://doi.org/10.1093/mnras/stad3516
Advance Access publication 2023 November 15

The Taurid Resonant Swarm at Mercury

Apostolos A. Christou [1]★ Auriane Egal [2,3,4] and Nikolaos Georgakarakos[5,6]

[1]*Armagh Observatory and Planetarium, College Hill, Armagh BT61 9DG, UK*
[2]*Planétarium de Montréal, Espace pour la Vie, 4801 av. Pierre-de Coubertin, Québec, Canada*
[3]*Department of Physics and Astronomy, University of Western Ontario, London, Ontario N6A 3K7, Canada*
[4]*IMCCE, CNRS, Observatoire de Paris, PSL Université, Sorbonne Université, Université de Lille 1, UMR 8028 du CNRS, 77 av. Denfert-Rochereau 75014 Paris, France*
[5]*Division of Science, New York University Abu Dhabi, Abu Dhabi, PO Box 129188, UAE*
[6]*Center for Astrophysics and Space Science (CASS), New York University Abu Dhabi, PO Box 129188, UAE*

Accepted 2023 November 9. Received 2023 November 9; in original form 2023 September 19

ABSTRACT

It has previously been suggested that ejection and vaporization of Hermean surface material by meteoroids from comet 2P/Encke causes a seasonal enhancement in Mercury's Ca exosphere observed by the NASA *MESSENGER* spacecraft in 2011-2015. The ESA/JAXA *BepiColo*en mission, now route*ute* to Mercury, will likely provide the next set of observational tests of this hypothesis after it enters orbit in late 2025. Here we study the Taurid Swarm Complex (IAU Code: STS), a population of cm-sized or larger meteoroids from Encke's comet that encounters the Earth every 3–7 yr. Through analysis of previous observations of the STS and many-particle numerical simulations, we study the circumstances of encounters between the STS and Mercury and find that, unlike the Earth where STS encounters is observed in some years but not others, each time the STS is at perihelion it encounters Mercury on three consecutive planetary orbits. We further predict that the STS will encounter this planet during the early stages of *BepiColombo*'s orbital mission. The temporal flux profile during each encounter will be broad and possibly double-peaked with total number fluence 0.4×–1.7× that of the sporadic fluence for >1 kg meteoroids on the sub-radiant hemisphere of the planet. The meteoroid arrival direction and sub-radiant point strongly depend on True Anomaly Angle, switching from mainly nightside to mainly dayside impacts as Mercury travels from orbital perihelion to aphelion. Our predictions may be used to create detailed models of exosphere generation by Encke stream meteoroids.

Key words: meteorites, meteors, meteoroids – methods: numerical – methods: data analysis – planets and satellites, individual: Mercury – comets: individual: 2P/Encke.

1 INTRODUCTION

Since the first close scrutiny by the *Mariner 10* spacecraft in the 1970s, it has been known that the planet Mercury is host to a tenuous atmosphere, produced by the complex interplay between processes that are generic to atmosphere-less bodies with solid surfaces (Killen et al. 2007; Wurz et al. 2010). The MErcury Surface, Space ENvironment, GEochemistry, and Ranging (*MESSENGER*) spacecraft operated at Mercury orbit from 2011 until 2015, allowing a close investigation of the Hermean exosphere. Measurements by the Mercury Atmospheric, and Surface Composition Spectrometer instrument characterized the temporal and spatial distribution of different exospheric species over ∼12 Hermean years, showing in particular that some species such as Ca follow a seasonal cycle (Burger et al. 2014). This was attributed to meteoroid bombardment and variations in the sporadic flux, but an additional source was required to reproduce the timing of peak Ca emission shortly after perihelion, at Mercury True Anomaly Angle (TAA) $\simeq 25^\circ$ (Killen & Hahn 2015). A suggested link between this feature and the stream of meteoroids released by comet 2P/Encke was investigated by Christou et al. (2015). This stream is relatively well-characterized due to its association with a number of distinct meteor showers at the Earth collectively known as the Taurid Meteoroid Complex (TMC; see e.g. Spurný et al. 2017; Egal et al. 2022b).

By modelling the Encke stream as a function of meteoroid size and age, it was found that mm-sized grains ejected from Encke $1 - 2 \times 10^4$ yr ago would intercept Mercury's orbit at the location of peak Ca emission. Subsequent modelling of both sporadic (Pokorný et al. 2017, 2018) and Encke stream flux (Egal et al. 2022b) on Mercury's surface have strengthened the case for a link between Encke and the post-perihelion Ca peak observed by *MESSENGER*, though the exact mechanism that injects the Ca in the exosphere is still under debate (Killen 2016; Plainaki et al. 2017; Moroni et al. 2023).

The next phase in the exploration of Mercury begins with the en route ESA/JAXA mission (Milillo et al. 2010) now en route to the planet where it is expected to arrive in late 2025. *BepiColombo* consists of two separate spacecraft, the Mercury Planetary Orbiter (MPO) and Mercury Magnetospheric Orbiter (MMO; now named 'Mio') that travel to Mercury attached to the Mercury Transfer

★ E-mail: apostolos.christou@armagh.ac.uk

Module (MTM). According to the mission plan[1] the spacecraft combination will remain within a few million km of Mercury following its 4th flyby of the planet in September 2024 until it finally enters orbit around Mercury at the 7th and final encounter on 2025 December 5. MPO and Mio will then separate from the MTM and prepare for their nominal one-Earth-year science mission when each spacecraft has reached their operational orbits.

Utilizing a diverse set of imagers & spectrometers, BepiColombo carries the promise of characterizing the Hermean environment & exosphere in greater detail than ever before. Of particular interest to meteoroid studies will be the SERENA instrument suite on *MPO* featuring the STROFIO mass spectrometry channel (Orsini et al. 2021) that should allow, for the first time, *in situ* detection of refractory and volatile species within plumes of ejecta generated by individual meteoroid impacts (Mangano et al. 2007), raising the prospect to constrain the large ($\gtrsim$0.1 m) meteoroid flux at Mercury from the BepiColombo observations.

The present work follows on from the Christou et al. (2015) study of the Taurid stream and the Hermean exosphere, focusing on a subpopulation of meteoroids from comet Encke collectively known as the Taurid Swarm Complex (TSC for short; Egal et al. 2022b). A distinguishing feature of the TSC is a high abundance of centimetre- to metre-sized meteoroids (with equivalent mass of several grams to 1000s of kg) producing episodes of increased fireball flux in the Earth's atmosphere (Asher & Izumi 1998; Dubietis & Arlt 2007; Olech et al. 2017; Spurný et al. 2017). We want to find out if the TSC is incident at Mercury particularly during BepiColombo's residence in Hermean space, as this would create an opportunity to obtain unique measurements of the effect of an already-characterized population of meteoroids on the planetary environment, on a par with an earlier campaign to monitor the upper atmosphere of Mars during the extremely close ($\sim 1.5 \times 10^5$ km) – and extremely rare – encounter of Oort-cloud comet C/2013 A1 (Siding Spring) with that planet in October 2014 (Tricarico 2015). Existing studies of the Hermean meteoroid environment (Cintala 1992; Marchi et al. 2005; Killen & Hahn 2015; Pokorný et al. 2017, 2018) have focused on the so-called sporadic population composed of dynamically evolved meteoroids that, in general, approach Mercury from different directions and at different speeds. In modelling the effects of a meteor stream such as the Taurids or the TSC on the exosphere of Mercury, we wish to highlight some important differences between sporadic and stream meteoroids. Specifically, the sporadic meteoroid radiants – the direction they would appear to arrive as seen from an observer at Mercury – are distributed over the entire sky (though not necessarily isotropically). In contrast, meteoroids in streams follow near-parallel paths and appear to arrive from a common radiant direction. The angle between the common stream radiant and the solar direction as seen from the planet is the solar elongation angle (SEA) that determines the relative number of impacts on the dayside and nightside (Fig. 1). The projections of this angle on the planetary orbital plane and on the orbit normal determine the sub-radiant latitude and Local Solar Time (LST) on Mercury. Since many of the candidate mechanisms that control the production and detectability of exospheric species depend on the presence of sunlight, the analysis presented in this work includes these important parameters and their time variation to inform future modelling of exosphere production.

[1]*BepiColombo* fact sheet: https://www.esa.int/Science_Exploration/Space_Science/BepiColombo/BepiColombo_factsheet. Published 2017-07-06. Retrieved 2023-07-27.

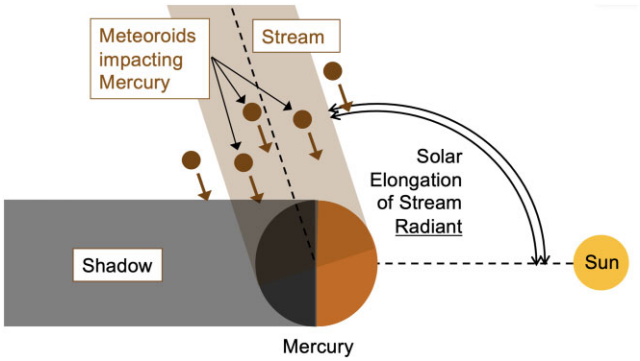

Figure 1. Geometric representation of the solar elongation of the radiant of a meteoroid stream.

This paper is organized as follows: in the further section we review available information on the TSC component of the Encke stream complex and its pertinent characteristics. In Section 3, we introduce a simple geometrical model of the TSC and address its intermittent nature, where a historically successful approach in predicting TSC encounters with the Earth is adapted to predicting the times of Mercury encounters. The geometric model is expanded upon in Section 4, aided by analysis of precisely measured TSC fireball orbits and by many-particle numerical simulations, to characterize the TSC structure and verify its gross features at Mercury. Section 5 is devoted to estimating the particle fluence and comparing it to other populations of Mercury-impacting meteoroids while Section 6 presents our detailed predictions for the next TSC encounter in 2025–26. Finally, in Section 7 we list our main conclusions.

2 THE TAURID SWARM (STS)

Not to be confused with the TMC, the TSC is a subpopulation of meteoroids associated with comet 2P/Encke in an orbit similar to the comet's but with a slightly higher semimajor axis. An orbital resonance between the meteoroids and Jupiter acts to azimuthally confine the material within an arc of some $\sim 80^\circ$ in mean anomaly, so that the Earth may encounter the TSC on some years but not others (Asher & Clube 1993; Asher & Izumi 1998; Dubietis & Arlt 2007; Egal et al. 2022b, see also Appendix A of this work). The mode and timing of TSC formation are uncertain but may be linked to fragmentation events of one or more progenitor bodies 5–7 kyr ago injecting some tens of 0.1–1 km NEAs in Encke-like, Earth-crossing orbits (Asher et al. 1993; Egal et al. 2021; Egal et al. 2022b).

Apart from its intermittent appearance, two other defining characteristics of the TSC are (i) an enhancement, by a factor or $2.4 - 4.6\times$, in the rate of bright fireballs from cm-sized and larger meteoroids at the Earth (Dubietis & Arlt 2007) thought to arise from the azimuthal confinement of material in the resonance with Jupiter, and (ii) the lack of smaller grains (Egal et al. 2022a) caused by gradual, size-dependent loss of material by radiation forces (Asher 1991). Due to the low, $\sim 5^\circ$ orbital inclination, the TSC encounters the Earth on both the inbound (October–November) and outbound (June–July) legs of its orbital path around the sun. Autumn branch meteoroids arrive at Earth from the antisolar direction, therefore most optical observations concern this night-time branch. Observational characterization of the Summer branch is generally hindered by the small SEA of the TSC radiant and by the lack of small meteoroids that radar surveys are more sensitive to. Specifically for the CMOR radar, overdense echoes are deliberately removed (Egal et al. 2022a) meaning Taurid

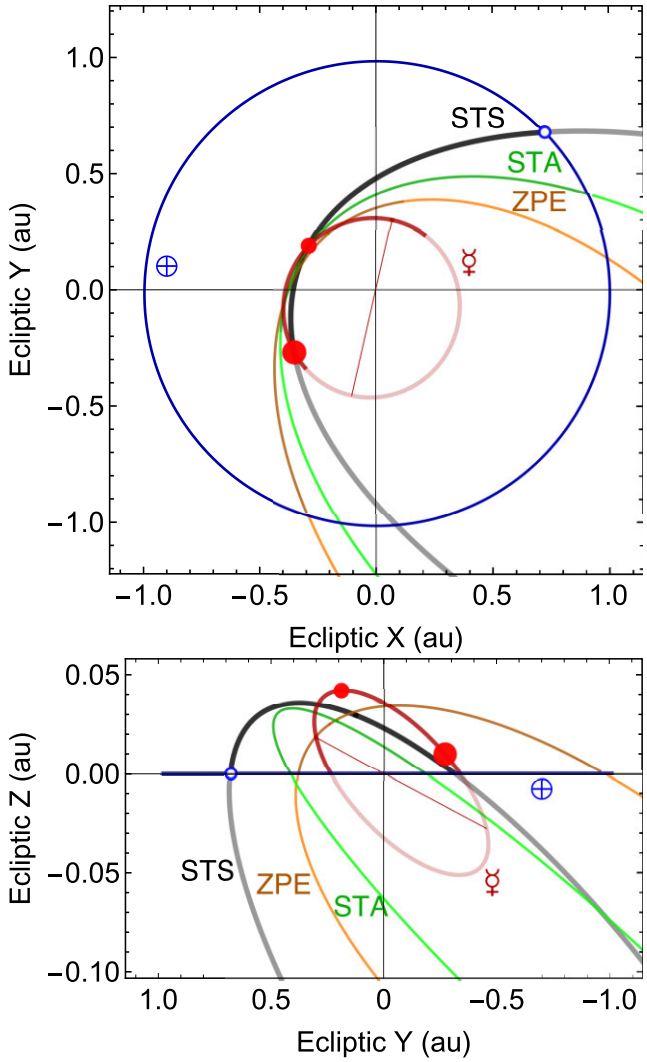

Figure 2. Orbits of the Earth, Mercury, and the s-Taurids referred to the ecliptic plane (*top*) and to the plane normal to the ecliptic X axis (bottom). Also included are the STA and ZPE showers. Orbit arcs below the ecliptic plane are shown with a lighter colour. The open symbol indicates the November STS crossing of Earth's orbit while the solid red points represent minima of the Mercury-STS distance (equation 1).

fireballs should not be present in the data at all. The Summer branch is also believed responsible for an unusually high rate of kg-class or larger meteoroids impacting the Moon in June 1975 (Duennebier et al. 1976). The TSC was recently introduced to the IAU Meteor Data Centre Working list of meteor showers as the s-Taurids (Shower #628; IAU 3-letter code: STS; Jenniskens, Nénon et al. 2016). Precise observations of STS fireballs recorded during the 2015 return (Olech, Zoladec et al. 2017; Spurný et al. 2017; Devillepoix et al. 2021) allowed to verify the STS location in the 7:2 resonance with Jupiter and to estimate the mass flux of STS meteoroids in the centimetre-to-metre range.

3 MERCURY-STS ENCOUNTER GEOMETRY

All geometric calculations in this Section use the STS orbit derived from analysis of CAMS data (Devillepoix et al. 2021). Fig. 2 shows this orbit together with the ζ Perseid (ZPE) and Southern Taurid (STA) orbits determined from Canadian Meteor Orbit Radar

Table 1. Orbital elements of the STS from Devillepoix et al. (2021) and of the principal TMC meteor showers and parent comet from Egal et al. (2022a).

Object id	a (au)	e	I (°)	ϖ (°)	Ω (°)
STS	2.237	0.847	5.45	158.4	42.72
SSO†	2.256	0.847	11.9	160.2	334.2
2P/Encke	2.215	0.848	11.78	161.1	334.6
NTA	2.180	0.825	2.9	158.4	227.5
BTA	1.910	0.812	2.9	159.1	275.4
STA	1.820	0.813	5.0	142.4	24.5
ZPE	1.610	0.804	5.4	130.3	73.5

Note.†Orbit of STS 'Source Object' from Asher & Clube (1993).

(CMOR) observations (Egal et al. 2022a, Table 1). Note that the longitudes of pericentre ϖ of Encke, the β Taurids (BTA) and Northern Taurids (NTA) are within ∼3° of each other, while those of ZPE and STA lag 20°–30° behind. These two latter showers are considered dynamically older populations within the TMC with the ZPE in particular produced no later than 16 kyr ago (Egal et al. 2022b). The Mercury-encountering Encke dust identified in Christou et al. (2015) as causing the observed peak in surface Ca vaporization rate most likely corresponds to these dynamically evolved meteoroids that, due to the apsidal lag and smaller semimajor axis, cross Mercury's orbit closer to its perihelion than other TMC showers (Fig. 2). The STS meets the orbit of Mercury above the ecliptic plane a few days from perihelion. By minimizing the orbit-to-orbit distance as a function of the respective TAAs:

$$\Delta(f, \mathrm{TAA}) = |\boldsymbol{r}_{\mathrm{STS}}(f; a, e, I, \omega, \Omega) - \boldsymbol{r}_M(\mathrm{TAA}; a_M, e_M, I_M, \omega_M, \Omega_M)|, \quad (1)$$

where the set (a, e, I, ω, Ω) denotes the orbital semimajor axis, eccentricity, inclination, argument of perihelion and longitude of ascending node, $\boldsymbol{r}$ is a position vector, and the 'M' subscript refers to Mercury, we identified two local minima (red points) with Δ_1=0.0099 au at TAA = 69° and Δ_2=0.0063 au at TAA = 140°, the second minimum being close to the stream's and to Mercury's descending nodes on the ecliptic plane. As the smaller value, Δ_2 is the current Minimum Orbit Intersection Distance (MOID; eg Carusi & Dotto 1996) between the orbits. These minima may be thought of as the counterparts of the Autumn and Summer branches at Earth though here they are closer together. At both locations, the planetocentric speed at encounter is ∼24 km s^{-1}, somewhat slower than at the Earth (∼29 km s^{-1}) but also to the Mercury Taurids (Christou et al. 2015). The difference is caused by the gradual shrinking of the orbits of mm-sized non-resonant TMC meteoroids by radiation forces that then intersect Mercury's orbit more transversely than STS. Because of the near-tangential encounter geometry, STS meteoroids may meet Mercury over a wide arc of its orbit with the planet outbound from perihelion towards aphelion.

To determine the epochs when Mercury encounters STS we follow Asher & Clube (1993), replacing the position of the Earth in their model with that of Mercury. The procedure is described in Appendix A and can be applied to an arbitrary Solar system body with a known orbit that intersects the STS orbit. The results are listed in Table 2 and further discussed in Section 6 where we present details of the next encounter between Mercury and STS. A search for observational evidence of past STS encounters at Mercury in the observational record is beyond the scope of the present work but we note here that Encounter #10 took place between April and December 2012 while MESSENGER was operating in Mercury orbit.

Table 2. Epochs given in the format YY/MM/DD between 1980/01/01 and 2040/01/01 when the STS is near perihelion. The number in brackets is the time difference between perihelion passages of Mercury and the STS.

ID	$M_{SC} = 0°$	$M_{SC} = -40°$	$M_{SC} = +40°$	Mercury at perihelion
1	82-02-17	81-10-02	82-07-04	82-01-23 (−25d)
2	85-07-08	85-02-21	85-11-23	85-06-07 (−31d)
3	88-11-27	88-07-13	89-04-14	88-10-21 (−37d)
4	92-04-18	91-12-02	92-09-02	92-03-05 (−42d)
5	95-09-07	95-04-23	96-01-23	95-10-16 (+ 39d)
6	99-01-27	98-09-12	99-06-14	99-02-28 (+ 32d)
7	02-06-18	02-01-31	02-11-02	02-07-14 (+ 26d)
8	05-11-06	05-06-22	06-03-24	05-11-27 (+ 21d)
9	09-03-28	08-11-10	09-08-12	09-04-11 (+ 14d)
10	**12-08-17**	**12-04-01**	**13-01-01**	**12-08-25 (+ 8d)**
11	16-01-06	15-08-22	16-05-23	16-01-08 (+ 2d)
12	19-05-28	19-01-10	19-10-12	19-05-24 (−4d)
13	22-10-17	22-06-01	23-03-03	22-10-06 (−11d)
14	**26-03-07**	**25-10-21**	**26-07-23**	**26-02-19 (−16d)**
15	29-07-27	29-03-11	29-12-11	29-07-05 (−22d)
16	32-12-16	32-07-31	33-05-02	32-11-17 (−29d)
17	36-05-06	35-12-21	36-09-21	36-04-02 (−34d)
18	39-09-26	39-05-11	–	39-08-16 (−41d)

4 DETAILED STS STRUCTURE AT MERCURY

Though useful in a pedagogical sense, the concept of the STS as a 1D string of meteoroids moving along a common Keplerian orbit introduced in the previous section is oversimplified in its assuming a vanishingly small stream cross-section. The observational record shows that the Earth takes some weeks to cross the STS, an equivalent cross-section of ∼0.1 au. The observed lateral extent of STS at the Earth is probably caused by dynamical evolution of the individual meteoroid orbits since their ejection. Moreover, we calculate here that meteoroids on the STS orbit would pass ∼0.08 au below the Earth's orbit on the outbound leg, suggesting that STS must also extend by a similar distance in the direction normal to the ecliptic in order to account for Summer branch observations such as the 1975 lunar impacts. To capture sufficient complexity in our modelling to allow quantitative predictions, we turn to analysis of recently acquired fireball orbital data and combine it with many-particle numerical simulations.

4.1 Constraints from the 2015 fireball observations

Spurný et al. (2017) presented a set of orbits for ∼200 multi station Taurids recorded by the European Fireball Network (EFN) during the 2015 STS return, of which 113 fireballs were classified as STS members. During the same period, 73 STS fireballs were recorded by the Australian Desert Fireball Network (ADFN) (Devillepoix et al. 2021) which we further filtered here to exclude orbits with $a<2$ au or $\sigma_a>0.05$ au, leaving 55 entries most likely to be STS members.

The fireball orbits from these data are plotted in Fig. 3. The orbits encounter the Earth on the ascending node, with the ADFN set (top panel) extending at slightly higher nodal values than the EFN set (bottom panel). The perihelia of these late-arriving fireballs lie outside Mercury's orbit and would most likely miss the planet.

The distributions of MOID, speed and solar elongation for the ADFN and EFN fireballs are shown in Fig. 4 where we denote in black those orbits that lie outside that of Mercury. The remaining orbits cross Mercury at TAA of 50°−90° and 120°−170° and with MOID between 0.003 and 0.014 au. Note also there are very few fireball orbits approaching Mercury between TAA=90° and TAA = 120°. Since the spatial extent of the STS should be larger than its Earth-encountering component, it is likely that STS actually encounters Mercury at or near those locations and additionally that those meteoroids have orbits similar to the Earth-crossing counterparts. The encounter speed and radiant SEA of these fireballs strongly depend on the TAA. As Mercury travels from perihelion (TAA=0°) to aphelion (TAA=180°), the solar elongation (middle panels) decreases monotonically from SEA=180°, that is, particles arriving from the antisolar direction, to SEA=0° where particles now arrive from the solar direction. At the same time, the encounter speed (bottom panels) decreases from 40 km s^{-1} near perihelion to

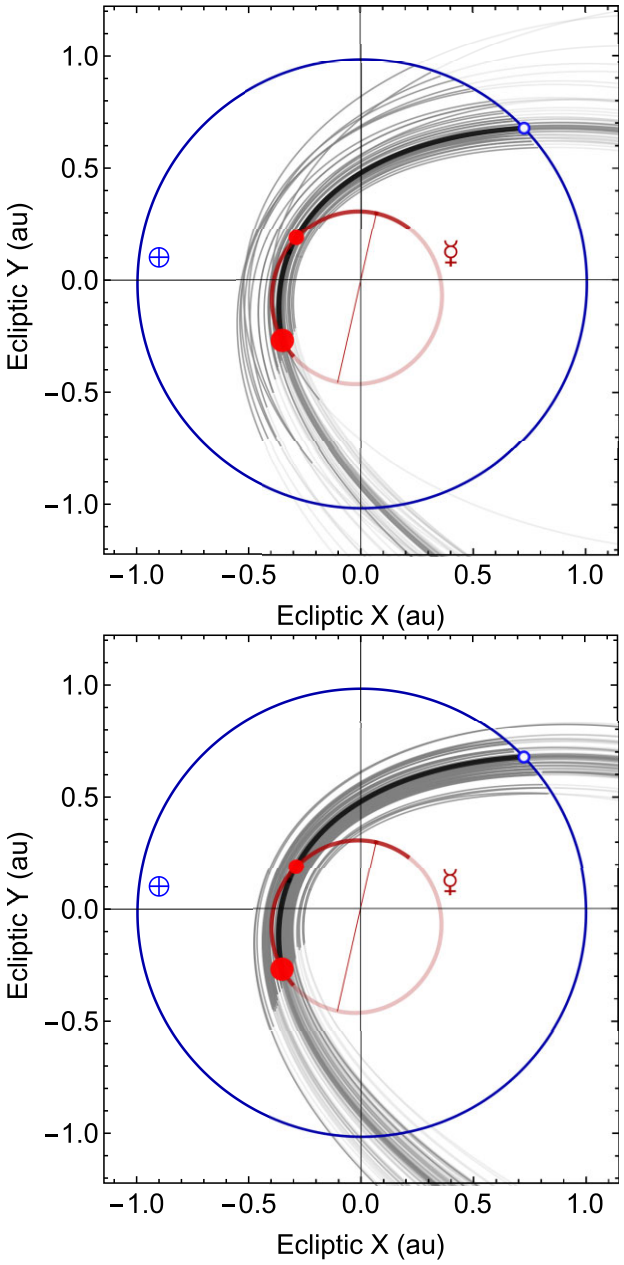

Figure 3. Orbits of STS fireballs from Devillepoix et al. (2021) (top) and from Spurný et al. (2017) (bottom) projected on the ecliptic plane. Solid red points and an open blue symbol are used as in Fig. 2 to indicate the orbital locations of minima in the Mercury-STS distance (equation 1) and of the November STS crossing of the Earth's orbit, respectively.

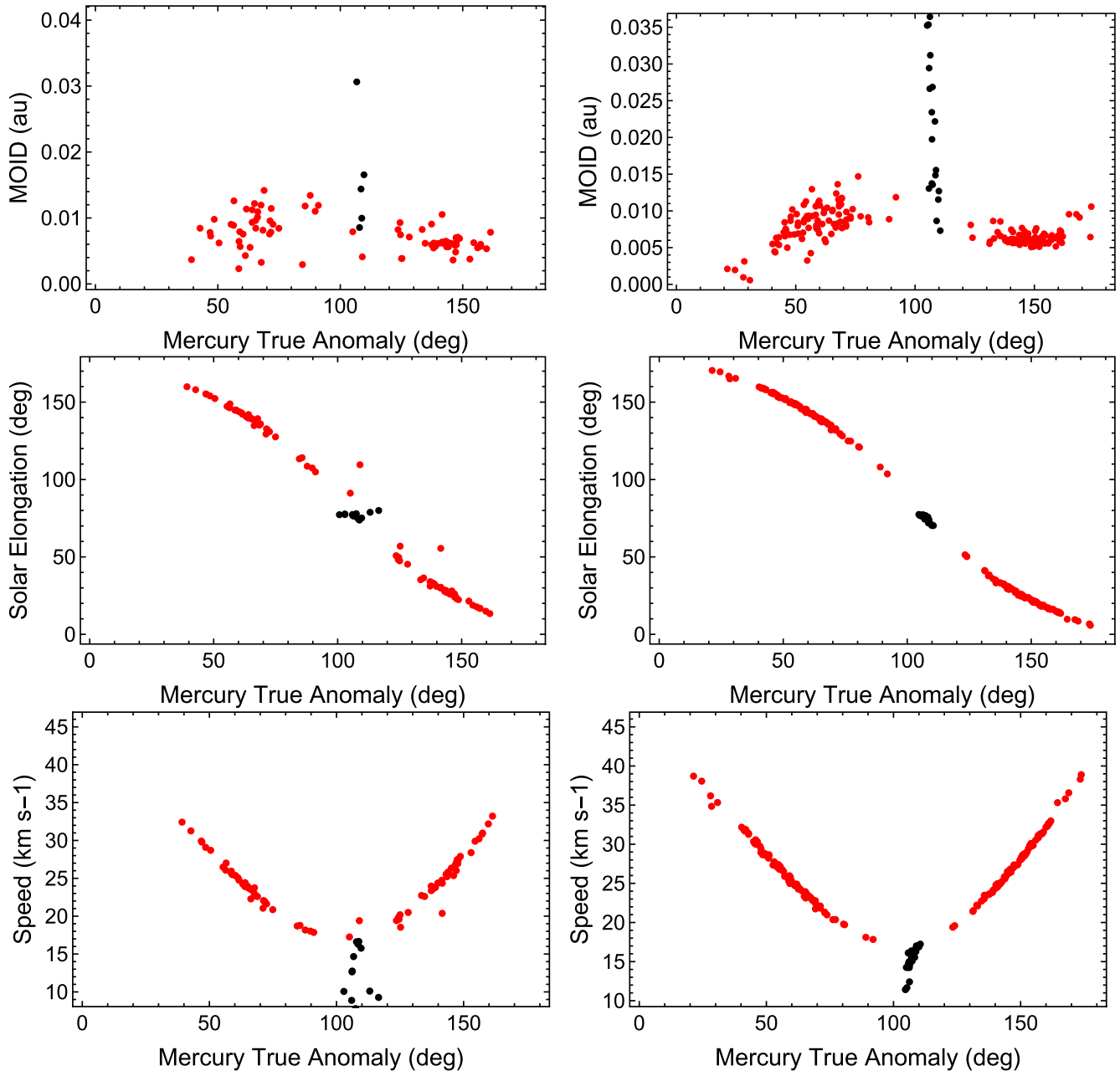

Figure 4. MOID (top), radiant solar elongation (middle), and speed (bottom) of STS fireballs in Fig. 3 at Mercury as functions of the TAA with the ADFN data (Devillepoix et al. 2021) shown in the left column and EFN data (Spurný et al. 2017) in the right column.

$15 - 20\,\mathrm{km\,s^{-1}}$ at TAA$\simeq$110°, then increasing again to $40\,\mathrm{km\,s^{-1}}$ near aphelion. The strong correlation between arrival time and orbital properties is also a feature of STS at the Earth (Spurný et al. 2017) and, as we shall see in the next section, it is also reproduced by our numerical simulations.

4.2 Constraints from numerical simulations

In studying the possible dynamical history of comet 2P/Encke, Egal et al. (2022b) identified one particular ephemeris of the comet with a specific, fixed set of values for the non-gravitational force component magnitudes – designated 'clone A4' – that successfully reproduces many of the observed characteristics of all four main Taurid complex showers (NTA, STA, BTA, and ZPE) simultaneously as the outcome of sublimation-driven meteoroid ejection from a cometary nucleus. That model was found to also reproduce the intensity and timing of STS returns at Earth (Asher & Izumi 1998) except that it anticipates by 4–8d the November arrival of STS fireballs. A unique property of clone A4 is its long residence time in the 7:2 resonance with Jupiter, with the critical angle

$$\phi = 7\lambda_J - 2\lambda - 5\varpi, \tag{2}$$

where λ is the mean longitude and ϖ the longitude of pericentre of the comet, librating around $\phi \simeq 0$ for $\sim$25 kyr during the last 30 kyr. Here we have carried out new simulation runs to explore further the link between the residence of the STS parent body in the resonance and the observed properties of STS at Earth. These new simulations are described in Appendix B and show that orbits with similarly

long residence time in the resonance consistently produce Earth-crossing streams with characteristics very much like the observed Taurids, strengthening the case for a long (10 s of kyr) residence time of the STS parent in this resonance. To then determine the TSC encounter circumstances at Mercury, we filter the particle final states from the Egal et al. numerical model to retain only particles with $D \geq 1$ cm presently in the 7:2 resonance having a MOID with Mercury below 0.02 au and within ± 10 d of Mercury being at the longitude of the MOID, thus ensuring that the particles physically approach the planet.

Fig. 5 shows the present states of STS particles ejected from clone A4 no earlier than 10 000 BCE (Before the Common Era; referred to years that came before the birth of Jesus Christ) separately from those of older particles. We observe that the distribution of these two populations along Mercury's orbit is generally different. The number frequency of younger particles (black points) is highest at TAA$\simeq$60° and at $\simeq$150°, offset by $\sim$10° and 5°, respectively from the local minima calculated using equation (1) (red-dashed lines). The respective distributions of SEA and speed at Mercury are identical to those of STS fireballs, including the gap at 90°<TAA<110°. Alternatively, older particles (grey points) encounter Mercury during the entire outbound half of the orbit. The locations of peak number frequency of these older particles are shifted towards the planetary apses as their higher dispersion on the STS orbital plane causes them to meet Mercury near the Mercury-STS nodes at TAA $= -11°$ & 169° (blue-dashed lines). A minor increase of the number frequency observed between 90° and 110° is most likely caused by the merging of the two red points in Figs 2 and 3 for particles that evolved to orbits exactly tangent to that of Mercury.

As already noted in our analysis of the fireball data, the arrival speed and solar elongation of the particles are strongly correlated with the TAA. The similarity in the frequency distributions for resonant and non-resonant particles (top panel of Fig. 5 and Egal et al. 2022b, Fig. H.1, respectively) further suggests that these relationships are valid for the annual – that is, non-resonant – component of the Taurids investigated in Christou et al. (2015) and Egal et al. (2022b) as well as the STS component. Since these parameters enter into model calculations of the impact-generated exosphere, we have binned the data every 10° in TAA and report in Appendix C the statistical means of the speed, the SEA and its projections both onto and normal to Mercury's orbit plane for every bin that contains >100 particles.

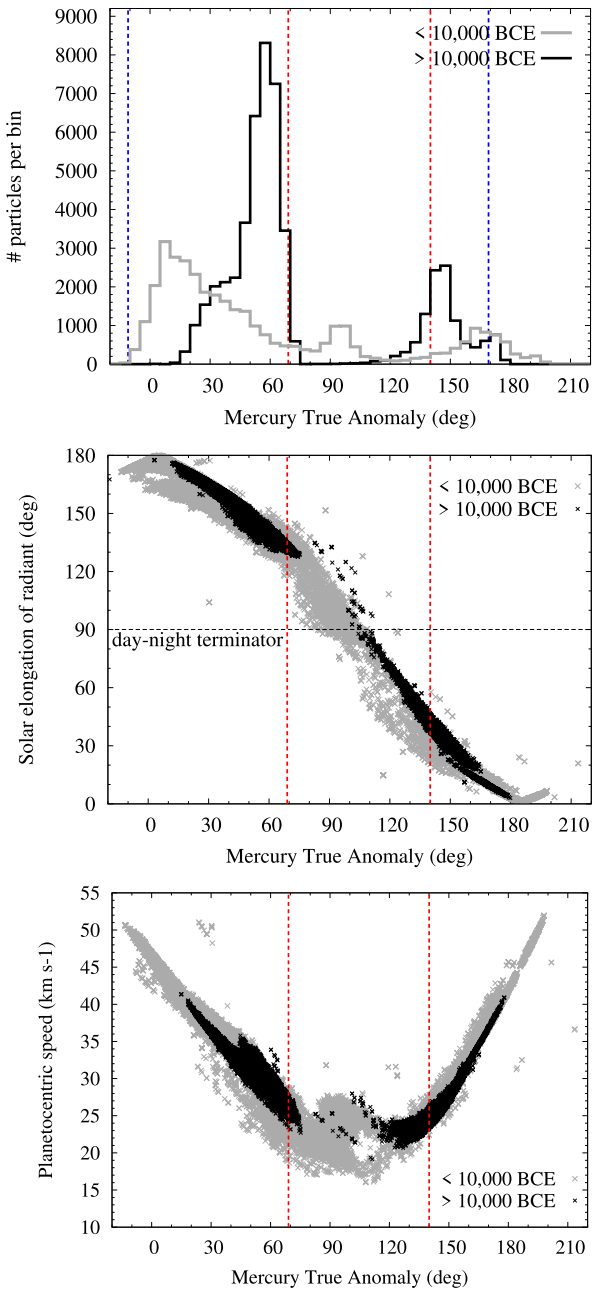

Figure 5. Top: Number frequency of resonant particles at Mercury ejected from 2P/Encke clone A4 before and after 10 000 BCE against the TAA. Middle: Solar elongation of the individual particle radiants. A radiant on the day-night terminator boundary (horizontal-dashed line; SEA = 90°) implies that 50 per cent of particles impact on the nightside and the other half on the dayside. Bottom: Particle impact speed. These distributions are similar to those of recorded STS fireballs (Fig. 4).

5 STS FLUENCE AT MERCURY

Ignoring the effect of gravitational focusing and acceleration near the planet, the respective STS meteoroid fluences at Mercury and the Earth are related by the expression

$$N_M(.) = (R_M/R_E)^2 (v_M/v_E) N_E(.), \tag{3}$$

where $R_{[.]}$ are the planetary radii and $v_{[.]}$ the planetocentric speeds. Devillepoix et al. (2021) used observations of the 2015 STS return by the CAMS network to estimate the number fluence $N^*(> m)$ of STS meteoroids at the top of the atmosphere as

$$\log_{10} N^*_{\rm TSC}(> m) = a_E - b_E \log_{10} m, \tag{4}$$

with $a_E = 5.15$, $b_E = 0.94$ when m is expressed in grams. To correct the fluence for gravitational acceleration and focusing, we write

$$N(.) = \left[1 + \left(\frac{v_{\rm esc}}{v_\infty}\right)^2\right]^{-3/2} N^*(.), \tag{5}$$

where v_∞ is the theoretical speed outside the planetary gravity field and $v_{\rm esc}$ the escape velocity. From Section 4, we have $v_{M,\infty} \simeq v_{E,\infty} \sim$ 30 km s^{-1} so applying equation (5) with $v_{E,\rm esc} = 11.2$ km s^{-1}, $v_{M,\rm esc} = 4.3$ km s^{-1} and substituting in equation (3) with $R_E =$ 6378 km and $R_M = 2440$ km yields

$$N^*_M(> m) \simeq 0.12 N^*_E(> m) \tag{6}$$

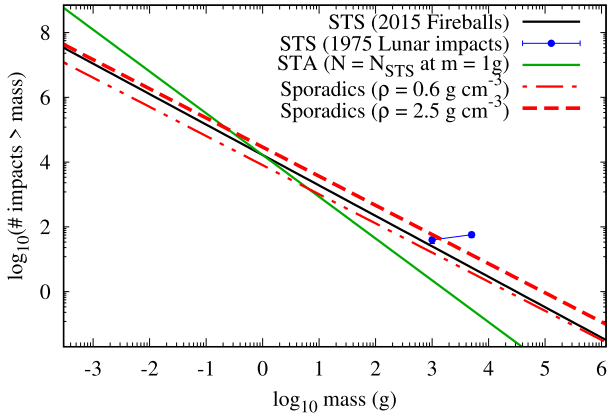

Figure 6. Number fluence at Mercury for different impactor populations as a function of meteoroid mass.

allowing to obtain the STS fluence at Mercury in the form of equation (4) with $a_M = 4.22$ and $b_M = 0.94$. We show this distribution in Fig. 6 together with the same distribution for the annual Taurids obtained from the STA magnitude distribution reported in Devillepoix et al. (2021) of their Fig. 4 and calibrated to match the STS distribution at $m=$ 1g. Interestingly, the slopes of these distributions straddle the value of -1 when mass is distributed evenly among equal logarithmic intervals. The steeper STA distribution places most of the stream mass in the smaller particles (Dohnanyi 1969; Pokorný et al. 2018), consistent with the Ca peak at TAA = 20°–30° in Mercury's exosphere being caused by mm-sized TMC meteoroids (Christou et al. 2015).

To compare these distributions with the sporadic flux at Mercury we use the model in Marchi et al. (2005) of the influx of asteroid belt debris expressed in terms of the meteoroid radius r:

$$h(r) = d\, r^{-e}\, \Sigma(\tau_c), \tag{7}$$

where $h(r)$ is the number of impacts by meteoroids of radius r metres per year and per unit impactor radius, d and e are constants and $\Sigma(.)$ is a numerical factor that depends indirectly on r through the collisional lifetime τ_c. For meteoroid sizes of interest in this paper, Σ varies between 0.08 and 0.11; here we fixed its value at 0.09. If we then consider that Mercury takes n days to cross the TSC, the equivalent sporadic fluence by meteoroids with radius $>r$ is

$$N_{\rm SP}(>r) = d^* r^{-e^*} \left(\frac{n}{365}\right), \tag{8}$$

with $d^* = 0.256$, $e^* = 2.7$. Evaluating equation (8) with $n = 365$ and $n = 1$ yields 1.7 impacts yr^{-1} for radii between 0.5 and 1.5 m, 2.2 impacts d^{-1} for $r = 0.05$–0.15 m and 149 impacts d^{-1} for $r = 0.01$–0.02 m, in excellent agreement with the fluxes calculated in Mangano et al. (2007). To compare the sporadic with the STS fluence (equation 4) we convert the radius dependence in the former expression to one of mass through the relationship

$$r = \left[m \Big/ \left(\frac{4}{3}\pi\rho\right)\right]^{1/3}, \tag{9}$$

where ρ is the meteoroid bulk density and we have also set $n = 20$ in equation (8) for consistency with the 2015 fireball observations.

Fig. 6 shows sporadic particle fluences at Mercury for different values of meteoroid bulk density: $\rho = 0.6\,{\rm g\,cm^{-3}}$ used to evaluate the strength of P–R drag on cometary dust in our new simulations (Appendix B), and $\rho = 2.5\,{\rm g\,cm^{-3}}$ for so-called 'astronomical silicates' (Dermott et al. 2001) and close to the value of $3.0\,{\rm g\,cm^{-3}}$ used in Mangano et al. (2007) with the 0.1m- and 1m-radius impactors discussed in that work corresponding to masses of 13 and 1300 kg, respectively. Blue points correspond to the 1975 lunar seismic detections (Duennebier et al. 1976; Oberst & Nakamura 1991) where the error bars represent 1σ Poisson counting statistics and are comparable to the symbol size. These two data points correspond to the same raw data but with different calibrations of the relationship between seismic amplitude and impactor properties. The point closer to the 2015 fireball data was calibrated against fireball orbital and flux information obtained by the Prairie network and MORP optical surveys (McCrosky et al. 1978; Halliday, Blackwell & Griffin 1984; Oberst & Nakamura 1989). The 1975 and 2015 STS data (with ΔM=+1° & −7°, respectively) are in reasonable agreement, providing us with an approximate but otherwise robust constraint on few-kg class STS impactors near the centre of the STS arc where one might expect the highest number density of material.

The similar slopes of the STS and sporadic distributions can be understood if they both represent collisionally derived populations (Marchi et al. 2005; Devillepoix et al. 2021) while the STA particles were produced by sublimation-driven ejection from a cometary nucleus (Egal et al. 2022b).

Using a meteoroid mass lower limit of 1 kg as a benchmark, we estimate an STS Mercury number fluence of ∼25 and a sporadic fluence 0.6×–2.3× the TSC fluence depending on the assumed meteoroid bulk density. Absolute fluence values for >13 kg meteoroids similar to those studied in Mangano et al. are 2.2 (STS) and 1.6–5.8 (sporadic), respectively. The fluence at masses ≫1 kg is less certain than implied by Fig. 6 due to the generally low number of recorded events caused by the most massive STS meteoroids. For instance, Devillepoix et al. (2021) estimate a fluence of 0.37 meteoroids >940 kg at the Earth during the 2015 STS which, if extrapolated at Mercury yields 0.044 impacts by tonne-class meteoroids during an STS encounter compared to 0.03 − 0.12 impacts by sporadics. The estimated Earth fluence is consistent with three (3) metre-sized bolides in 2005 and 2015 identified by those authors in archival data collected by US Government (USG) satellite sensors in geostationary orbit as likely STS members. Alternatively, two confirmed s-Taurid bolides of estimated masses of 30 and 1300 kg detected by the EFN in 2015 (Spurný et al. 2017), though statistically consistent with the USG detections, also allow a much higher (a few 100×) fluence of 10^3 kg class STS meteoroids due to the much smaller atmospheric detection area of the EFN network.

Additional sources of model uncertainty derive from our assumed effective duration of the shower where, for instance, setting $n = 10$ instead of $n = 20$ in equation (8) effectively doubles the STS fluence relative to sporadics. Note also that the actual relative strengths of the two activity peaks in Fig. 5 may vary from those in our numerical model, as they depend on the (unknown) activity profile and dust productivity of the comet thousands of years ago, on the size distribution of ejected grains and on the ejection mechanism itself. Moreover, different geometric constraints apply to sporadic and stream meteoroid impacts so that, for instance, parity in the flux per unit area between sporadics and the STS would double the number of impacts on the sub-radiant hemisphere of the planet during the STS encounter but not affect the anti-radiant hemisphere. Finally, the sporadic flux at Mercury, though not mono-directional as a cometary stream would be, is likely far from isotropic (Marchi et al. 2005; Pokorný et al. 2017, 2018) making interpretation of both flux and fluence measurements of the different meteoroid populations at Mercury dependent on the ability to localize those impacts.

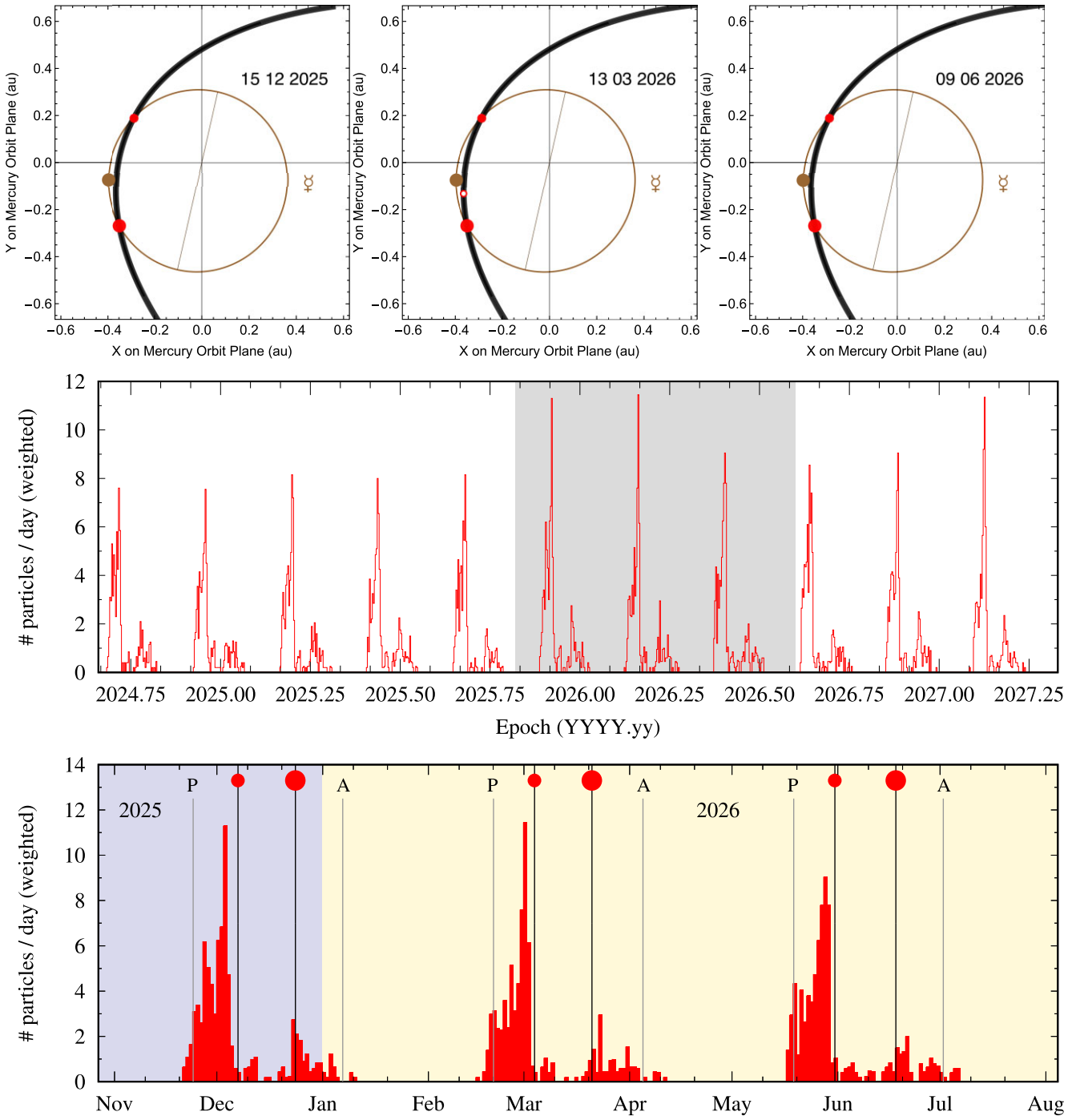

Figure 7. Top: Snapshots from three consecutive encounters between the STS (thick black arc) and the planet Mercury (brown symbol) in December 2025 (top left), March 2026 (top centre) and June 2026 (top right). Mercury is physically close to the STS centre (open red symbol) during the 2nd encounter. Middle: Daily counts of particles that approached Mercury between September 2024 and May 2027 in our simulations. Bottom: Detail of middle panel (shaded area) highlighting the three encounters between STS and Mercury. Times when Mercury is at perihelion ('P') or aphelion ('A') are indicated by the grey vertical lines. Tick marks along the horizontal axis correspond to the 1st, 10th and 20th days of each month.

Table 3. Predicted epochs of peak STS flux at Mercury in 2025–26.

	Encounter #1	Encounter #2	Encounter #3
Mercury@Δ_1	2025 Dec 05	2026 Mar 03	2026 May 30
Mercury@Δ_2	2025 Dec 23	2026 Mar 21	2026 June 17

6 THE 2025-26 MERCURY-STS ENCOUNTER

The STS will next pass through perihelion between late 2025 and mid-2026 (Entry #14 in Table 2). During that period, Mercury will encounter the STS on three consecutive orbits while outbound from perihelion and from November until January (Encounter #1), February until April (Encounter #2) and May until July (Encounter

#3) (Fig. 7, top). At each encounter, our numerical model predicts up to two separate peaks in STS flux ∼18 d apart with the exact dates given in Table 3. The February-to-April encounter occurs when the centre of STS (open symbol, top centre panel) is near perihelion ($\Delta M \simeq 0^\circ$) and physically close to the planet. Table 2 shows that such encounters occur when Mercury reaches perihelion about a quarter orbit (∼22 d) before the STS centre (last column) and this set of circumstances recurs every 40 yr or so, the last time being in the 1980s. If we assume that the two peaks in Fig. 5 yield comparable fluxes of meteoroids, total meteoroid fluence during the encounter period should be $\lesssim 2\times$ that shown in Fig. 6. Impacts will initially (TAA $\sim 0^\circ$) be incident on the night-time hemisphere and gradually migrate across the afternoon side of the planet to yield pre-dominantly daytime impacts when TAA $\sim 180^\circ$ (Fig. 5). Impact speeds at the peak epochs are $25-30\,\mathrm{km\,s^{-1}}$ and somewhat higher ($35-45\,\mathrm{km\,s^{-1}}$) for any STS meteoroids arriving at Mercury near the orbit apses. The other two encounters occur when $\Delta M = \pm 25^\circ$, still within the TSC but further from the centre. The particle fluence on those locations is less well constrained by observations and, in the absence of strong evidence to the contrary, we postulate that it is similar to that at the February–April encounter.

Note that particles in our simulations are also seen approaching Mercury both before and after the three highlighted encounters in Fig. 7, middle panel. These particles are likely also trapped in the 7:2 resonance with Jupiter but do not correspond to any actual material along the STS orbit. Indeed, we note that solutions between 0 and 2π to the equation $\phi(M) = 0$ with $\phi(.)$ from equation (2) come in pairs of angles 180° apart, however there is no observational evidence for material 180° across from the STS location.

Assuming BepiColombo operations follow the nominal mission plan, the first STS Encounter will occur near the time of Mercury Orbit Insertion, Encounter #2 as MPO and Mio maneuver independently to reach their operational orbits and Encounter #3 during the first months of the primary mission phase. As the next TSC crossing after 2026 will occur well after the primary scientific mission as well as the possible extended mission (Table 2), any scientific observations during these periods and especially Encounter #2 in February–April 2026 when Mercury is physically close to the STS centre offer a unique opportunity to characterize the STS at a location away from 1 au, its contribution to the large impactor flux at Mercury as well as the role of meteoritic impact vaporization as an exosphere source process. STS and the STA/ZPE components will generally approach Mercury at different LSTs than the bulk of sporadic meteoroids (Marchi et al. 2005; Pokorný et al. 2017, 2018) with the Encke dust avoiding the dawn hemisphere of the planet (Section 4 & Appendix C). This feature should help to separate out their contribution to the exosphere from the BepiColombo measurements while continued observations in subsequent Hermean years when the STS will be absent should allow to isolate and characterize the flux of the annually recurring Taurids and of sporadic meteoroids. Moreover, detecting and identifying STS meteoroid impacts would help constrain the formation age of the STS as the activity profile is apparently sensitive to this parameter (Section 4.2).

7 CONCLUSIONS AND DISCUSSION

This work investigated the incidence at Mercury of STS, a subpopulation of the 2P/Encke stream complex noted for its high abundance in gram-class or larger particles relative to the annual Taurids and was motivated by the prospect of observing the response of the Hermean environment to Taurid meteoroids *in situ* following the arrival of the BepiColombo twin-spacecraft mission to the planet. Our investigation benefits from new models of the Taurid stream and its different components (Egal et al. 2021; Egal et al. 2022b) as well as analyses of recent high-quality observations of the STS (Spurný et al. 2017; Devillepoix et al. 2021; Egal et al. 2022a).

Our main conclusions can be summarized in the following statements

(i) Mercury should encounter the STS just as it does the annual Taurids (Christou et al. 2015).

(ii) Encounters between Mercury and STS do not occur each time the planet crosses the STS orbit, mimicking in this way the STS intermittent appearance at the Earth. However, the encounters can still be predicted through a simple geometrical model similar to the one used previously to anticipate Earth-STS encounters (Asher & Clube 1993).

(iii) When STS is near perihelion, Mercury crosses it repeatedly during the post-perihelion half of its orbit. During each crossing the meteoroid flux, arrival geometry, and impact speed will vary with TAA.

(iv) The next STS encounter occurs between late 2025 and mid-2026, during the early stages of BepiColombo's orbital mission at Mercury.

Measurements by the different instruments onboard BepiColombo's two component orbiters should provide direct observational verification of meteoroid models and elucidate the nature of their relation to the exosphere. The sporadic meteoroid model used in Mangano et al. (2007) and compared here against the annual and STS Taurid flux assumes that cm-sized or larger impactors originate from the Main asteroid Belt (MB). Recently, Pokorný et al. (2018) investigated the sporadic flux at Mercury for particle sizes smaller than a few mm using as starting point the zodiacal cloud model of Nesvorný et al. (2010). The 2018 study found that MB material are a minor contributor to Hermean impactors, with most of the mass fluence linked to cometary debris. Though the Marchi et al. (2005) and Pokorný et al. (2018) studies investigated different size regimes, they nevertheless both predict a collisionally evolved population of Mercury impactors with relatively shallow mass/size distribution slope. Therefore, the mass dependence of the sporadic source strength illustrated in Fig. 6 is probably a fair representation of the truth, at least for <1 g meteoroids. However, a cometary as opposed to an asteroidal origin would weaken the contribution of sporadics vs the STS & STA sources due to the lower density of cometary material. This should be observationally verified.

ACKNOWLEDGEMENTS

Astronomical research at the Armagh Observatory & Planetarium is grant-aided by the Northern Ireland Department for Communities (DfC). Discussions with Dr Rosemary Killen helped improve the presentation of results from our study. We would also like to thank the High Performance Computing Resources team at New York University Abu Dhabi and especially Jorge Naranjo for helping us with our numerical simulations. This work was supported in part by NASA Meteoroid Environment Office under cooperative agreement 80NSSC21M0073.

8 DATA AVAILABILITY

The data generated in this research are available from the corresponding author upon reasonable request.

REFERENCES

Asher D. J., 1991, PhD thesis, Oxford University
Asher D. J., Clube S. V. M., 1993, QJRAS, 34, 481
Asher D. J., Izumi K., 1998, MNRAS, 297, 23
Asher D. J., Clube S. V. M., Steel D. I., 1993, MNRAS, 264, 93
Burger M. H., Killen R. M., McClintock W. E., Merkel A. W., Vernack R. J., Jr, Cassidy T. A., Sarantos M., 2014, Icarus, 238, 51
Carusi A., Dotto E., 1996, Icarus, 124, 392
Chambers J. E., 1999, MNRAS, 304, 793
Christou A. A., Killen R. M., Burger M. H., 2015, Geophys. Res. Lett., 42, 7311
Cintala M. J., 1992, J. Geophys. Res., 97, 947
Dermott S. F., Grogan K., Durda D. D., Jayaraman S., Kehoe T. J. J., Kortenkamp S. J., Wyatt M. C., 2001, in Interplanetary Dust. Springer-Verlag, Heidelberg, Germany, p. 569
Devillepoix H. A. R., et al. 2021, Planet. Sci. J., 2, id.223
Dohnanyi J. S., 1969, J. Geophys. Res., 74, 2531
Dubietis A., Arlt R., 2007, MNRAS, 376, 890
Duennebier F. K., Nakamura Y., Latham G. V., Dorman H. J., 1976, Science, 192, 1000
Egal A., Wiegert P., Brown P. G., Spurný P., Borovička J., Valsecchi G. B., 2021, MNRAS, 507, 2568
Egal A., Brown P. G., Wiegert P., Kipreos Y., 2022a, MNRAS, 512, 2318
Egal A., Wiegert P., Brown P. G., 2022b, MNRAS, 515, 2800
Giorgini J. D., et al., 1996, Bull. Am. Astron. Soc., Vol. 28, p. 1158
Halliday I., Blackwell A. T., Griffin A. A., 1984, Science, 223, 1405
Jenniskens P., et al. 2016, Icarus, 266, 331
Killen R. M., 2016, Icarus, 268, 32
Killen R. M., Hahn J. M., 2015, Icarus, 250, 230
Killen R., et al., 2007, Space Sci. Rev., 132, 433
Mangano V., Milillo A., Mura A., Orsini S., De Angelis E., Di Lellis A. M., Wurz P., 2007, Planet. Space Sci., 55, 1541
Marchi S., Morbidelli A., Cremonese G., 2005, A&A, 431, 1123
McCrosky R. E., Shao C. Y., Posen A., 1978, Meteoritica, 37, 44
Milillo A., et al. 2010, Planet. Space Sci., 58, 40
Moroni M., et al. 2023, Icarus, 401, id. 115616
Nesvorný D., Jenniskens P., Levison H. F., Bottke W. F., Vokrouhlický D., Gounelle M., 2010, ApJ, 713, L816
Oberst J., Nakamura Y., 1989, Proc. Lunar Planet. Sci. Conf., 19, 615
Oberst J., Nakamura Y., 1991, Icarus, 91, 315
Olech A., et al. 2017, MNRAS, 469, 2077
Orsini S., et al. 2021, Space Sci. Rev., 217, 11
Plainaki C., et al. 2017, JGR: Planets, 122, 1217
Pokorný P., Sarantos M., Janches D., 2017, ApJ, 842, L17
Pokorný P., Sarantos M., Janches D., 2018, ApJ, 843, L31
Spurný P., Borovička J., Mucke H., Svoreň J., 2017, A&A, 605, id.A68
Tricarico P., 2015, Geophys. Res. Lett., 42, 4752
Wurz P., Whitby J. A., Rohner U., Martin-Fernandez J. A., Lammer H., Colb C., 2010, Planet. Space Sci., 58, 1599

APPENDIX A: THE ASHER & CLUBE ΔM MODEL APPLIED TO MERCURY

The quantity ΔM in Asher & Clube (1993), the time difference by which the planet misses the STS centre, is formally defined as

$$\Delta M = M_{\rm SC} - M_{\rm PE}, \tag{A1}$$

where $M_{\rm SC}$ is the location of the STS centre, $M_{\rm PE}$ is the location of the planet at encounter and $M_{\rm PE}$ can be calculated if the STS orbit and the planetary orbit are known. To test the sensitivity of $M_{\rm PE}$ to the input orbit, we calculated it for the different orbits listed in Table 1 as well as for the 'source object' orbit in Asher & Clube (1993) cf their Table V. For the STS orbit in Devillepoix et al. (2021) we obtain $M_{\rm PE}$=−12°.3 for the Autumn branch crossing of Earth's orbit. This number varies by up to 0.3° if orbits from Table 1 with semimajor axis differing by a few $\times 10^{-2}$ au are used instead, namely that of 2P/Encke and the orbit from Asher & Clube. For NTA we find −13°.1 and for the remaining orbits (BTA, ZPE, and STA) we obtain values between −16° and −21°. Since the STS semimajor axis is constrained by the resonant condition to lie between 2.23 and 2.28 au, we adopt $M_{\rm PE} = -12^\circ$ in the calculations that follow.

The mean anomaly of the STS centre may be expressed as

$$M_{\rm SC} = M_0 + n_{\rm SC} * (t - t_0)\,, \tag{A2}$$

where $n_{\rm SC} = a_{\rm SC}^{-3/2}$ and $t - t_0$ is in years. Setting $a_{\rm SC} = 2.256$ au and adopting the values of t_0 and M_0 for the year 1988 we are able to recover the model values of ΔM (Table B1; see also Fig. A1). To apply the model to Mercury, we require that STS is at perihelion, that is

$$M_{\rm PE} = 0, \tag{A3}$$

representing the two close approach points in Fig. 2 located at $M_1 = -1^\circ$ and $M_2 = +3^\circ$, respectively.

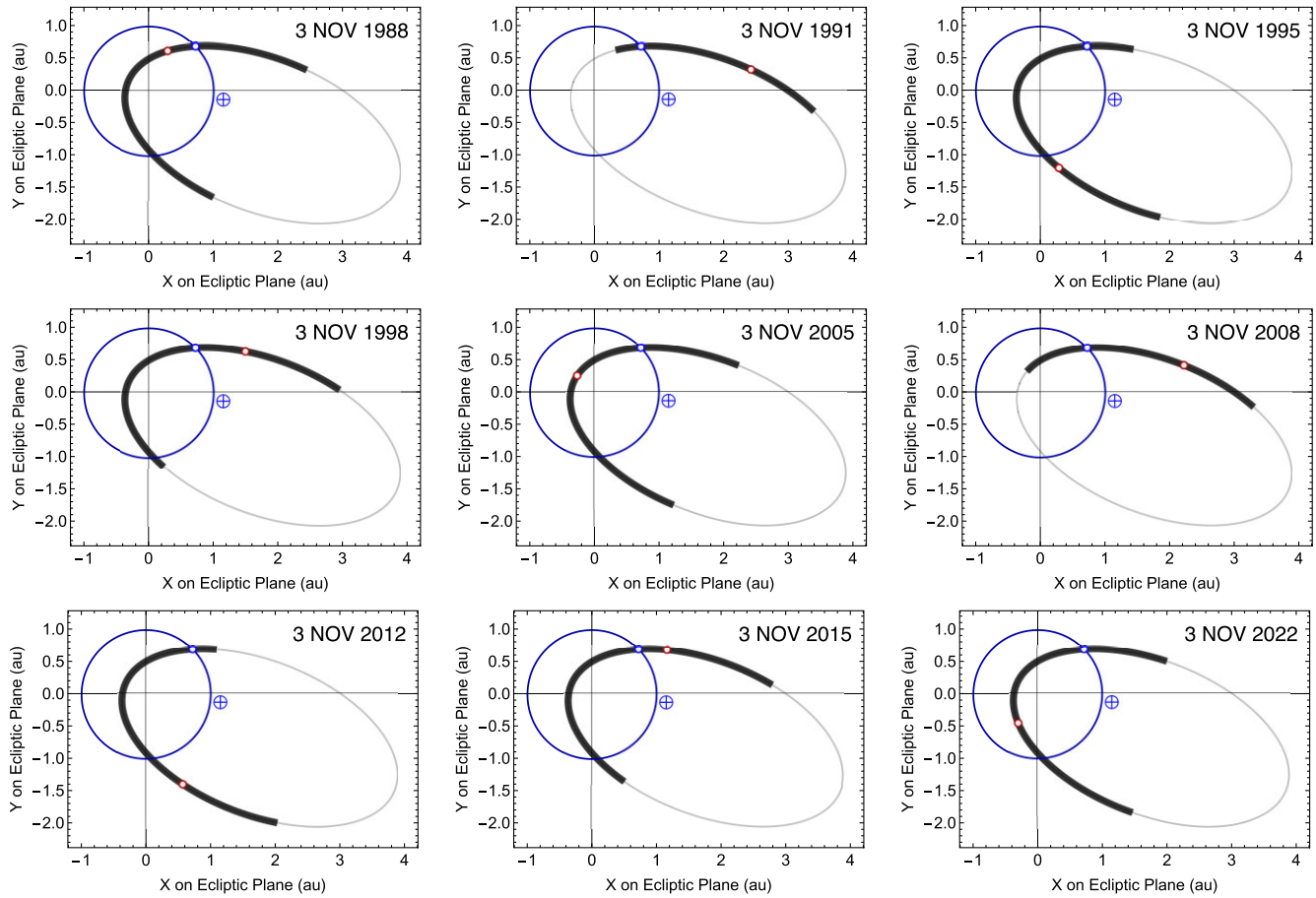

Figure A1. Illustration of STS encounters with Earth from Table B1 used to test the ΔM model with STS shown as a thick black orbital arc. The blue and red open symbols indicate Earth's location on 3 November of each year and the centre of the STS respectively.

APPENDIX B: NEW SIMULATIONS OF STS FORMATION

To additionally test the robustness of the model predictions, we generated a new model of the STS by first back-integrating the orbit of A4 under the specific non-gravitational force parameters used in Egal et al. and the HYBRID symplectic state propagation

Table B1. Data from Asher & Clube (1993) used to test the retrieval of M_{SC} from equation (4). Each line entry refers to 3 November of the corresponding year.

Epoch	ΔM (deg)
1988	**+5**
1991	−36
1995	+29
1998	−13
2005	+11
2008	−30
2012	+35
2015	−7
2022	+17

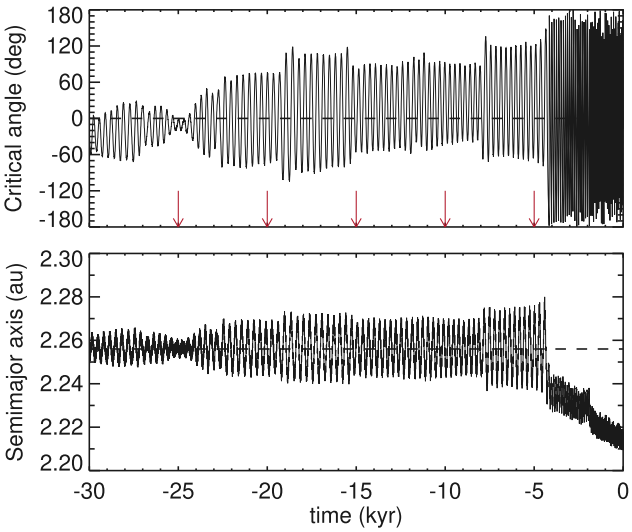

Figure B1. Evolution of the critical angle ϕ (top) and semimajor axis a (bottom) for clone A4P1 used in our new STS simulations. Dashed horizontal lines are drawn at $\phi = 0$ and $a = 2.256$ au, respectively. Vertical arrows indicate the epochs when particles are ejected from the reference orbit.

Table B2. Starting orbits for the simulations of STS formation from clone A4P1.

Designation	Epoch (JD)	Semimajor axis (au)	Eccentricity	Inclination (°)	Argument of perihelion (°)	Longitude of ascending node (°)	Epoch at pericentre (JD)
−25k	−6679707.0	2.25650121	0.89336478	15.77491436	351.73509	15.19280	−6679366.422657
−20k	−4853455.0	2.26077878	0.88955223	12.34723485	200.93725	283.76848	−4853049.898871
−15k	−3027207.0	2.25659361	0.88756925	3.86698686	140.69906	280.87069	−3027064.037345
−10k	−1200955.0	2.24756425	0.87871901	16.52104272	355.35969	95.89758	−1200599.789237
−5k	625293.0	2.27343730	0.86337778	7.23128035	200.63073	283.76848	625489.359431

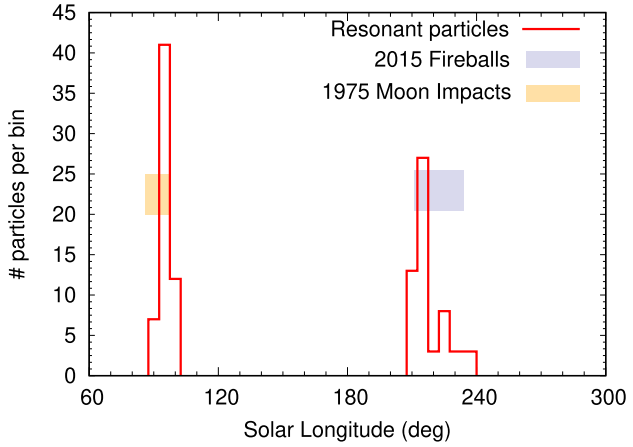

Figure B2. Particles ejected from Encke clone A4P1 between 5 and 15 thousand years ago that encountered Earth in the last 1000 yr. The orange and blue boxes correspond to recorded STS encounters with the Earth-Moon system in 1975 and 2015 as described in the text.

scheme within the MERCURY6 package (Chambers 1999) with a 4-d time step with a Solar system model comprising the eight major planets. Initial planetary state vectors were obtained from the HORIZONS online ephemeris service (Giorgini et al. 1996) at the J2000 epoch. We observed that the semimajor axis of A4 increased going backwards in time, crossing the location of the 7:2 resonance at $t \simeq -6000$ yr without being trapped in it. This is not unexpected as the use of different integrators or planetary ephemerides may result in a completely different dynamical history for this comet (Egal et al. 2022b, A4 ephemeris available online at: https://data.mendeley.com/datasets/6rrwfvzbx5/2).

By manual inspection, we found that the clone with initial semimajor axis differing from A4 by $\Delta a = +10^{-4}$ au became trapped and spent ∼25 kyr in the 7:2 resonance (Fig. B1), a finding consistent with the reported 1-in-7 upper limit on the relative abundance of Encke clones in the Egal et al. investigation spending at least a few millenia in the resonance during the last 30 kyr. This new dynamical clone of comet Encke, which we refer to here as 'A4P1', was selected as the reference for our modelling of the STS at Earth. Batches of 1000 test particles were ejected from the reference orbit at perihelion at 5000 yr intervals (Table B2) and with speed uniformly sampled between 0 and 10 m s^{-1} both along and against the direction of motion. The particle states were propagated forward in time with a force model that included Poynting–Robertson (PR) drag and radiation pressure (RP) for particle diameters $D = 0.1$, 1, and 5 cm and a density $\rho = 0.6\,\mathrm{g\,cm^{-3}}$, similar to the value of $1.0\,\mathrm{g\,cm^{-3}}$ used in Egal et al. (2022b) and corresponding to the following values for the non-gravitational force parameter β (Dermott et al. 2001): 1.9×10^{-3}, 1.9×10^{-4} and 3.8×10^{-5}. Simulation runs with PR & RP switched off ($\beta = 0$) were also carried out to model the evolution of larger meteoroids. The thermal Yarkovsky effect was not considered in these simulations.

Fig. B2 shows solar longitude distributions for particles with $D > 1$ cm in our −5k, −10k, and −15k runs encountering Earth no earlier than 1000 yr ago, compared to arrival times of STS fireballs from Devillepoix et al. (2021) and Spurný et al. (2017) on the Autumn branch as well as the 1975 lunar impact events (Duennebier et al. 1976) on the Summer branch. There is excellent overall agreement between our simulation and the observations. We note that the 2015 fireballs (light-blue box) lead the peak flux from our model by a few days while a similar offset in the opposite direction is hinted at for the Summer branch and the lunar data (orange box). Interestingly, the former feature resembles the offset noted by Egal et al. (2022b) between the A4 STS model and the Devillepoix et al. (2021) fireball data.

APPENDIX C: DETAILED PREDICTIONS FROM THE EGAL ET AL NUMERICAL MODEL.

In Table C1 we tabulate statistical means of speed and solar elongation data from the numerical simulations of Egal et al. (2022b) binned every 10° in TAA. The Hour Angle (HA) quantity is related to the LST of the sub-radiant point with HA=0° placing it at local noon while HA=±180° places it at local mid-night.

Table C1. Planetocentric speed, solar elongation, ecliptic latitude, and sun-relative hour angle (HA) of the Mercury sub-radiant point for different particle populations in Egal et al. (2022b).

	Ejected after 10k BCE				Ejected between 10k & 20k BCE			
TAA (°)	v (km s^{-1})	SEA (°)	Lat. (°)	HA (°)	v (km s^{-1})	SEA (°)	Lat. (°)	HA (°)
0	–	–	–	–	45	176	2	−174
10	–	–	–	–	43	174	4	169
20	39	170	1	171	40	168	9	172
30	36	165	5	166	37	159	16	166
40	33	157	11	161	35	151	23	162
50	32	145	24	155	32	144	27	155
60	29	139	29	150	27	138	23	146
70	27	134	31	144	24	133	15	137
80	–	–	–	–	22	118	−10	120
90	–	–	–	–	24	100	−44	104
100	–	–	–	–	24	93	−50	94
110	24	85	−50	82	23	78	−40	75
120	23	69	−42	61	22	55	−26	51
130	23	54	−33	46	23	41	−13	39
140	25	41	−24	34	26	31	−12	28
150	27	32	−18	26	29	25	−13	21
160	32	19	−9	16	34	18	−13	12
170	37	9	−3	8	38	11	−8	7
180	40	5	−2	5	41	4	−2	3
190	–	–	–	–	47	3	−1	−3

This paper has been typeset from a TEX/LATEX file prepared by the author.